The effect of thermal fluctuations on elastic instabilities of biopolymers

Emanuel, M.D.

Chapter 5

Plectoneme formation of double-stranded DNA under torsion

5.1 Motivation

We will now extend the WLC model to include the response to torsional stresses in the chain. The helical structure of dsDNA makes the understanding of supercoiling, under torsional stress, important for the mechanics of transcription and replication in both prokaryotes and eukaryotes. Torsion induced supercoiling is also thought to be an important ingredient for the compactification of DNA into the bacterial nucleoid. Also here was it the introduction of single molecule techniques, that made it possible to examine the torsional response of DNA in a precise and controlled way. Making use of the preferred direction for its magnetic moment of super paramagnetic beads [95], allows to measure the relation between torsion and extension while using a force clamp. Also with optical tweezers torsion can be applied while stretching DNA [145], using specially fabricated beads. For larger tensions micropipettes have been used [146]. Since the first magnetic tweezer experiments the precision in measurement has increased to a level that makes it possible to resolve many open questions concerning the elastic properties of DNA. Next to these measurements of the extension as a function of the linking number several methods have been used to measure at the same time the torque [145, 147].

A large amount of models have been devised to describe these experiments, from purely mechanical models [148], mechanical models with electrostatic interactions [149, 150] models that include some entropic effects [151] to phenomenological models [152], each targeted to explain some feature in a specific experiment. Our goal is to make a model built from first principles, valid over a large range of monovalent salt concentrations and loading forces. Our approach differs in several aspects from previous work. First of all we take explicitly the full chain as a continuous elastic rod into consideration. We will show that the writhe of the

chain can be calculated exactly. The electrostatic interaction we take with some precision into account following [153] and argue why this approach is correct.

It is clear that some approximations and simplifications are unavoidable to keep the model simple enough to handle; we will nonetheless capture the essential features that the measurements reveal. In this chapter we introduce the ingredients of the model as an extension of the WLC model from Chapter 3. We will explain the way the plectoneme is formed while being connected to the tails in Section 5.2. In Section 5.4 we will review the various interactions that play a role in the formation of a plectoneme in some detail.

5.2 The mechanistic Plectoneme

Again we describe dsDNA as a persistent chain, for length scales above the helical repeat of 3.5 nm. Since the chain is not torsion free in these experiments, its ends rotationally constrained, we follow the ribbon approach of the previous chapter.

It has to be stressed that we hide the local twist of the double helix in the definition of the ribbon. This twist does show up in a twist stretch coupling, that surprisingly turns out to be negative [154, 151]: twist increases with increasing tension. Its measured value is $-21\,k_BT$ [155]. The stretch modulus of dsDNA is rather high, with values in the literature of around 1200 pN [96, 151]. Its direct influence on the extension is small for the forces we are interested in (up to 4 pN). The negative twist stretch coupling has due to this also only a minor influence on the experiments. In this chapter we will not take them into account to avoid clogging the expressions too much. Both we will include when we discuss the influence of thermal fluctuations in Chapter 7.

The energy density of the chain consists of four parts: the bending energy, the twist energy, the potential energies of the externally applied force respectively the torque, and the non-local volume interactions. The Kirchhoff analogy states that this system, without volume interactions, can be mapped to that of a spinning top, whose Hamilton density is the Lagrange density of the elastic ribbon. Since we assume that the chain has an isotropic circular cross-section, the system is mapped to the Lagrange case, which is classically integrable, i.e. a complete set of integrals of motion exists. A comprehensive overview and classification of its solutions can be found in [156].

In the realms of classical elasticity, neglecting thermal fluctuations, applying a torque on a ribbon under tension does at first not change the shape of the centerline up to a critical torque where a buckling bifurcation is reached schematically depicted in Figure 5.1, similar to the buckling transition under compression of an elastic rod as introduced in Chapter 3. At this critical torque loops will form that, constrained by non-local volume interactions, finally will release twist into a plectoneme until the energy gain in releasing twist equals the energy cost of the resulting plectoneme(s) (see Figure 5.2). It is generally assumed that the torque won't change after the nucleation and one speaks of the plectoneme torque as the final torque. The reasoning is that once a plectoneme has formed the increase in linking number all

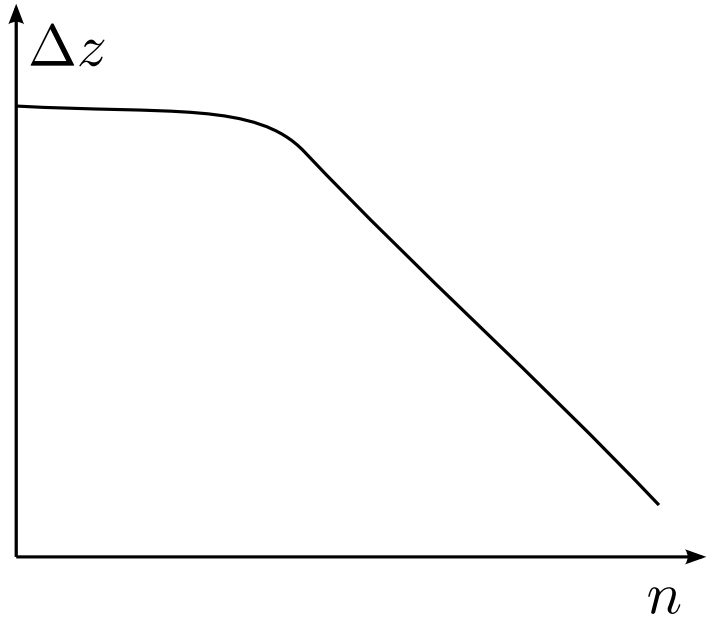

Figure 5.1: Sketch of a typical curve observed when twisting DNA under tension. n is the number of turns, Δz the extension of the molecule.

goes into a regular plectoneme. Since the twist does not change anymore, the torque, being proportional to the twist, should also be constant. This plectoneme torque can be calculated from the turn extension measurements by assuming the torque-linking number relation to be linear before the transition [145]. If indeed the torques does not change once a plectoneme is formed, the torque can be calculated using Maxwell relations between torque/linking number and force/extension [147]. In that last case the linear dependence below the transition is used only once under high tension. Oddly enough there is a discrepancy between the resulting plectoneme torques. This we will resolve in Chapter 7.

The mechanical cost of plectoneme formation caused by the bending of the strands into a helix favors a flat thin plectoneme, with a plectoneme angle $\alpha \simeq \pi/2$. However in this limit the writhe per plectoneme length, as we will soon discuss, is zero and there is no twist release possible. The most efficient twist release happens for $\alpha \simeq \pi/4$. The realized angle will be in between these two limits. The effect of electrostatic interactions is to slightly increase the angle as we will discuss in Section 5.4.3

In general the diameter of the plectoneme tends to be smaller than that of the loop, whose size is largely set by the tension. The optimal diameter of the plectoneme is the result of a competition between

1. efficiency in using contour-length for twist reduction, the cost growing linear with the tension.

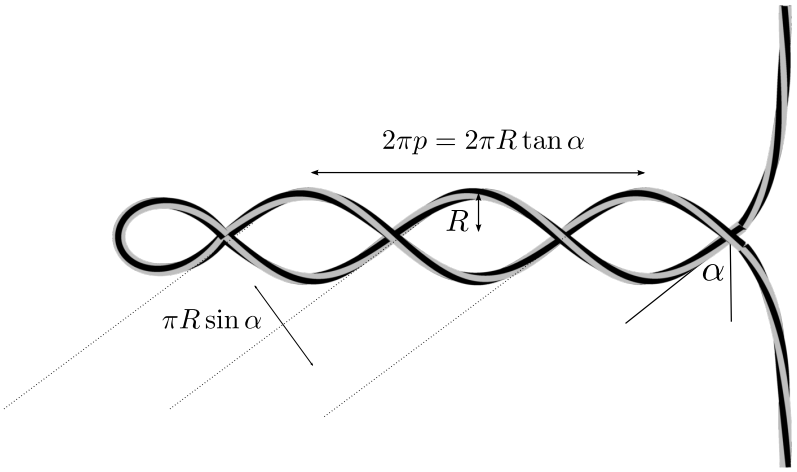

Figure 5.2: The shape of the WLC after buckling. The radius R of the plectoneme is measured from the centerlines of the opposing strands. The dsDNA radius sets a lower limit to this radius.

2. the resistance against bending, favoring a flat plectoneme.

3. electrostatic repulsion favoring a larger radius and plectoneme angle.

4. thermal fluctuations that drive the strands apart, mostly affecting the radius.

Increasing the number of turns after the buckling transition increases only the length of the plectoneme, since it is energetically favorable over twist increase. Thermal fluctuations cause the chain to tunnel to a plectoneme before the linking number has reached the bifurcation point. This is not the only thermal effect though. A thorough analysis of thermal fluctuations in the plectoneme turns out to be necessary. In Chapter 7 we will show how to take thermal fluctuations into account after plectoneme nucleation in a proper way under the relevant experimental conditions. This results in a prediction of a new phase in between the classic plectoneme phase and the chaotic chain, where plectoneme formation does not become favorable before the bifurcation point. The theory will be checked against extensive experiments from the Seidel group.

5.3 Linear elasticity

In the experiments using magnetic beads the force is fixed, the gradient of the magnetic field working as a force clamp. The linking number, the "number of turns" is controlled by a rotating magnetic field and the end to end distance of the chain is recorded as a function of these two control parameters. Adding twist and torsion, the reduced energy of the WLC can

be written as follows:

$$\mathcal{E} = \int_{-\mathrm{L_c}/2}^{\mathrm{L_c}/2} \mathrm{d}s \left[\frac{\mathrm{P_b}}{2} \dot{\mathbf{t}}^2(s) + \frac{\mathrm{P_c}}{2} \Delta\psi^2(s) - \mathrm{f} \cdot \mathbf{t}(s) \right] - 2\pi \, \mathrm{Lk}([\mathbf{t}, \Delta\psi])\tau_f + \mathcal{E}_{el}([\mathbf{t}]). \quad (5.1)$$

The torque along the force axis, τ_f, is a Lagrange multiplier in case the number of turns is used as a constraint. The linking number is a functional of the local coordinates of the model. The last term, the electrostatic contribution, is responsible for the volume interactions. We split the linking number into a twist and a tangential part using White's equation (4.7) from the last chapter. We write:

$$\begin{aligned} \mathrm{Lk}([\mathbf{t}, \Delta\psi]) &= \mathrm{Tw}([\Delta\psi]) + \mathrm{Wr}([\mathbf{t}]) \\ &= \frac{1}{2\pi} \int_{-\mathrm{L_c}/2}^{\mathrm{L_c}/2} \mathrm{d}s \Delta\psi(s) + \mathrm{Wr}([\mathbf{t}]). \end{aligned} \quad (5.2)$$

The use of Fuller's local expression is especially handy in the low torque regime, where one could hope that large fluctuations around the ground state, not allowing for writhe homotopy, are energetically suppressed enough to give a negligible contribution to the partition sum, but care has to be taken since the existence of a writhe homotopy can only be checked on a global scale. For a stability analysis, where we only look at infinitesimal fluctuations, it is fine though. We use polar coordinates for the tangent vector with the same choice as in Chapter 3:

$$\mathbf{t}(s) = (\cos\phi\cos\theta, \sin\phi\cos\theta, \sin\theta) \qquad \theta \in [-\pi/2, \pi/2], \phi \in [-\pi, \pi] \quad (5.3)$$

The map is again regular around the straight chain state, $\phi = \theta = 0$. The x-axis is chosen in the direction of the force. We now check when the energy functional has negative eigenvalues in its fluctuation determinant. The reference curve is the straight chain aligned along the x-axis. Its writhe we set to zero and it is a solution of the Euler-Lagrange equations. Fuller's equation (4.14) leads to:

$$\begin{aligned} \mathrm{Wr}(\{\phi, \theta\}) &= \frac{1}{2\pi} \int_{-L_c/2}^{L_c/2} \mathrm{d}s \frac{(\mathbf{e}_x \wedge \mathbf{t}(s)) \cdot \dot{\mathbf{t}}(s)}{1 + t_x(s)} \\ &= \frac{1}{2\pi} \int_{-L_c/2}^{L_c/2} \mathrm{d}s \frac{\sin(\phi(s))\dot{\theta}(s) - \cos(\phi(s))\sin(\theta(s))\cos(\theta(s))\dot{\phi}(s)}{1 + \cos(\phi(s))\cos(\theta(s))} \end{aligned} \quad (5.4)$$

The energy in these coordinates is:

$$\mathcal{E} = \frac{\mathrm{P_b}}{2}\int_{-\mathrm{L_c}/2}^{\mathrm{L_c}/2} \mathrm{d}s\left(\cos^2(\theta(s))\dot{\phi}^2(s) + \dot{\theta}^2(s)\right) + \frac{\mathrm{P_c}}{2}\int_{-\mathrm{L_c}/2}^{\mathrm{L_c}/2} \mathrm{d}s\Delta\psi^2(s) - 2\pi\tau_f\left(\mathrm{Wr}(\{\phi,\theta\}) + \frac{1}{2\pi}\int_{-L_c/2}^{L_c/2}\mathrm{d}s\Delta\psi(s)\right) + \mathrm{f}\left(\mathrm{L_c} - \int_{-\mathrm{L_c}/2}^{\mathrm{L_c}/2}\mathrm{d}s\cos(\phi(s))\cos(\theta(s))\right) + \mathcal{E}_{el}(\{\phi,\theta\}) \quad (5.5)$$

We use OSF [157, 158] theory to account for the electrostatic interactions through a renormalized persistence length and drop the electrostatic term. Fluctuations $\mathrm{d}\phi(s), \mathrm{d}\theta(s)$ on top of the straight chain contribute to a change in energy of:

$$\delta\,\mathcal{E} = \int_{-\mathrm{L_c}/2}^{\mathrm{L_c}/2}\mathrm{d}s\mathbf{X}^T(s)\hat{T}\,\mathbf{X}(s) \quad (5.6)$$

where we introduced

$$\mathbf{X}(s) = \begin{pmatrix}\delta\phi(s)\\ \delta\theta(s)\end{pmatrix} \qquad \hat{T} = \begin{pmatrix} -\frac{\mathrm{P_b}}{2}\frac{\mathrm{d}^2}{\mathrm{d}s^2} + \frac{\mathrm{f}}{2} & \frac{\tau_f}{2}\frac{\mathrm{d}}{\mathrm{d}s} \\ -\frac{\tau_f}{2}\frac{\mathrm{d}}{\mathrm{d}s} & -\frac{\mathrm{P_b}}{2}\frac{\mathrm{d}^2}{\mathrm{d}s^2} + \frac{\mathrm{f}}{2}\end{pmatrix}. \quad (5.7)$$

When $\tau_f \geq \sqrt{2\,\mathrm{f}\,\mathrm{P_b}}$ the determinant of $\hat{T}$ is minimized to a value of $\det\hat{T}$ for Fourier modes with a wavenumber of $k = \sqrt{\frac{\tau_f^2}{2\,\mathrm{P_b}^2} - \frac{\mathrm{f}}{\mathrm{P_b}}}$. The minimum reached is:

$$\det(\hat{T}) = \frac{\tau_f^2}{4\,\mathrm{P_b}^2}(\mathrm{f}\,\mathrm{P_b} - \frac{\tau_f^2}{4}) \quad (5.8)$$

When the torque (or the corresponding linking number) reaches a value of

$$\tau_{cr} = 2\sqrt{\mathrm{f}\,\mathrm{P_b}} \qquad \Longleftrightarrow \qquad n_{cr} = \frac{\sqrt{\mathrm{f}\,\mathrm{P_b}}L_c}{\pi\,\mathrm{P_c}} \quad (5.9)$$

the straight rod solution becomes unstable, as indicated by the sign change of the determinant, marking a transition to a configuration where twist has been traded in for writhe.

For an infinite chain the stable ground state above this *bifurcation point* is a helical shape [159], becoming localized when the boundary effects come into play. In the extreme case of an infinite long chain with tangents at infinity aligned along the direction of force, the solutions correspond to the homoclinic solutions of the equivalent (under the Kirchhoff analogy) symmetric top [156]. We will discuss them and then show that finite size corrections are negligible in the parameter regime we are interested in.

The general solutions of the elastic rod, with twist under a torque low enough that volume interactions do not play a role are characterized by 3 constants of motion in the Kirchhoff analogy. A common choice are the torque along the force direction, τ_f, the torque along the centerline, τ_3, or equivalently the rate of twist $\Delta\psi$, and the local Lagrange density. The homoclinic solutions are characterized by their asymptotic behavior:

$$\lim_{s\to\pm\infty} \mathbf{t}(s) = \mathbf{e}_z, \tag{5.10}$$

the main deviation from the straight chain is chosen around $s = 0$. Following [156] we choose the force along the z-axis and standard polar coordinates for the tangent. The Lagrange density reads:

$$\mathcal{L} = \frac{\mathrm{P_b}}{2}(\sin^2(\theta)\dot{\phi}^2(s) + \dot{\theta}^2(s)) + \frac{\mathrm{P_c}\,\Delta\psi^2}{2} + \mathrm{f}\cos\theta(s) \tag{5.11}$$

and the homoclinic solutions are given by:

$$\cos(\theta(s,t)) = 1 - 2t^2\,\mathrm{sech}^2(t\frac{s}{\lambda}) \tag{5.12}$$

$$\phi(s,t) = \arctan\left(\frac{t}{\sqrt{1-t^2}}\tanh(t\frac{s}{\lambda})\right) + \sqrt{1-t^2}\frac{s}{\lambda}, \tag{5.13}$$

where $\lambda = \sqrt{\mathrm{P_b}\,/\,\mathrm{f}}$ is again the deflection length. For each $t \in [0,1]$ the above equations define a homoclinic solution. This class of solutions defines at the same time the required homotopy of non crossing curves between the straight line at $t = 0$ and localized solutions up to any value of $t \in [0,1)$. The electrostatic potential keeps $t < 1$ and so we can use Fuller's equation with the z-axis as reference curve, resulting in a writhe of:

$$\begin{aligned}\mathrm{Wr_{loop}}(t) &= \frac{1}{2\pi}\int_{-\infty}^{\infty} \mathrm{d}s \frac{(\mathbf{e}_z \wedge \mathbf{t}(s))\cdot\dot{\mathbf{t}}(s)}{1+t_z(s)} \\ &= \frac{2}{\pi}\arcsin(t).\end{aligned} \tag{5.14}$$

These solutions indeed solve the Euler Lagrange equations, at an appropriately chosen torque, and their Lagrange density is constant along the contour. The energy of the homoclinic solutions has a potential contribution and equal elastic contribution that add to

$$\mathfrak{E}_{\mathrm{loop}}(t) = 2\,\mathrm{f}\,\mathrm{L_{loop}} \qquad \mathrm{L_{loop}} = \int_{-\infty}^{\infty} \mathrm{d}s\,[1-\cos(\theta(s,t))] = 4\lambda t. \tag{5.15}$$

with $\mathrm{L_{loop}}$ the change in extension compared to the straight chain, which we will use as the length of the loop part of the solution. This results in an energy of the homoclinic solution

with given linking number Lk:

$$\mathcal{E}(t) = \mathfrak{E}_{\text{loop}}(t) + \frac{(2\pi)^2\,\mathrm{P_c}}{2\,\mathrm{L_c}}\left[\mathrm{Lk} - \frac{2}{\pi}\arcsin(t)\right]^2. \tag{5.16}$$

From this expression follows that for tensions $\mathrm{f} < \mathrm{f_0} := 4\,{\mathrm{P_c}}^2/(\mathrm{P_b}\,{\mathrm{L_c}}^2)$ the energy minimum shifts from the straight rod continuously to the homoclinic loop when increasing the linking number from Lk_{cr} (5.9) till 1. For tensions above $\mathrm{f_0}$ only a limited range of stable solutions in between the two extremes exists. Also in that case the straight rod ceases to be stable at Lk_{cr}, while the barrier to the loop solution disappears a little later, when:

$$\mathrm{Lk} = \mathrm{Lk}_{cr}\sqrt{1 - \frac{4}{\mathrm{Lk}_{cr}^2\,\pi^2}} + \frac{2}{\pi}\arcsin\left(\frac{2}{\mathrm{Lk}_{cr}\,\pi}\right) \tag{5.17}$$

In Figure 5.3 a typical situation is sketched for a chain of 600 nm and a tensile force of 2 pN $\gg \mathrm{f_0}$. Note how already in an early stage a local minimum starts to form separated by a barrier from the straight rod that shifts to smaller t values with increasing Lk.

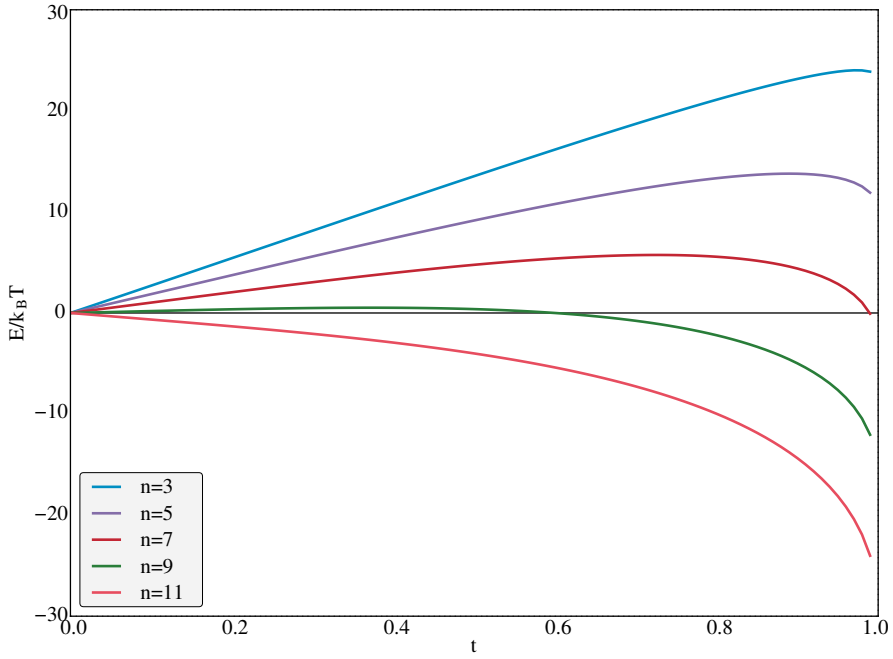

Figure 5.3: Relative energies of homoclinic solutions as a function of the homoclinic parameter t for several linking numbers, n. The energy is relative to the straight rod where all of the linking number is in the twist of the chain.

The excluded volume interactions, caused by short distance electrostatics, stabilize the final loop. At the moment this electrostatics dictated loop configuration has been reached, more twist will be released through plectonemic extension of the loop, discussed in the next section.

The two legs of the homoclinic solutions have a non trivial point of closest approach whenever $t > t_c \simeq 0.80424$. Its value is found from the nontrivial minimum of

$$d(s,t) = 2\lambda\sqrt{4t^2\,\mathrm{sech}^2(st/\lambda)\sin^2(s\sqrt{1-t^2}/\lambda) + (s/\lambda - 2t\tanh(st/\lambda))^2}. \qquad (5.18)$$

For a given force this distance has a maximum of $d_m \simeq 1.4\lambda$, for the critical homoclinic parameter t_c. This maximum has an important influence on the possibility of plectoneme formation, limiting the strength of electrostatics or the weakness of screening allowed, since as a condition for plectoneme nucleation one expects a point of closest approach, functioning as a pivot.

To separate the local OSF type effect of chain stiffening from the nonlocal loop destabilizing electrostatics the loop size should be larger than the Debije screening length [160]. It is possible to extend this approach over a larger range [161]. We have reasons not to do this:

1. The experimental conditions are such that the loopsize is considerably larger than the screening length. This is not accidental, since at the moment that they are almost equal a simple scaling argument would reveal that the energy cost per gained writhe in the plectoneme is in that case of the same magnitude as that of the loop. Combining this with the entropic gain in forming more loops, plectoneme nucleation is unlikely.

2. The details of the groundstate energetics of the endloop are not relevant for plectoneme formation even close to the transition point, when thermal fluctuations are taken into account.

3. It would complicate the calculations considerably without a benefit relevant to the measurements.

We will finally discuss finite size effects on the ground state solution space. By comparing the exact one loop solution for a finite chain with the homoclinic loop solution it is straightforward to shows that the energy increase, to lowest order, is given by:

$$\Delta\,\mathcal{E}_{\mathrm{finite}}(y) = 64\,\mathrm{f}\,\mathrm{L_c}\exp(-2\,\mathrm{L_c}\,/\lambda) \qquad (5.19)$$

Since in the experiments considered $\mathrm{L_c} >> \lambda$, this exponential decaying factor is negligible, until most of the chain sits in a plectoneme.

5.4 The Plectoneme

5.4.1 Geometry

After the formation of the homoclinic loop generically, depending on the salt concentration, a plectoneme will form, since as we will see the growing of a plectoneme is energetically cheaper than the formation of another homoclinic loop, to change twist into writhe.

The simplest model for electrostatic interactions would start from the repulsion of 2 parallel rods. As can be seen from Figure 5.2 it wouldn't do justice to the geometry of the plectoneme as was thoroughly discussed by Ubbink and Odijk [153]. The reason is that seen from one point along the chain, the electrostatic repulsion by the opposing strand has a radial component, increasing the plectoneme radius, and a pitch component, increasing the plectoneme angle, that are not equivalent.

We will for simplicity take the plectoneme radius and angle to be constant along the plectoneme, but take the homoclinic limit solution to be set by the demand that the nontrivial shortest distance between the two legs of the homoclinic solution, is equal to twice the plectoneme radius. It is here that we will define the start of the plectoneme, ending in the remaining part of the homoclinic solution, that remains connected rotating around the plectoneme with the growing plectoneme. In this way our solution is continuous. One could argue that the assumption of constant plectoneme parameters does not represent the true minimum of the free energy and that in reality the space curve should be smooth. However details of the energetics are not important for the experiments, where most contributions come from the plectoneme alone.

We will use the following space curve parameterized by the contour length s to describe a plectoneme starting at $s = 0$:

$$\begin{array}{ll} s \in [0, \mathrm{L_p}/2] : & s \in [\mathrm{L_p}/2 + \mathrm{L_{loop}}, \mathrm{L_p} + \mathrm{L_{loop}}] : \\ \mathbf{r}_p(s) = \begin{pmatrix} (s_0 + s)\sin\alpha \\ -R\cos\left((s_0 + s)\frac{\cos\alpha}{R}\right) \\ R\sin\left((s_0 + s)\frac{\cos\alpha}{R}\right) \end{pmatrix} & \mathbf{r}_p(s) = \begin{pmatrix} (s_0 + \mathrm{L_p} + \mathrm{L_{loop}} - s)\sin\alpha \\ R\cos\left((s_0 + \mathrm{L_p} + \mathrm{L_{loop}} - s)\frac{\cos\alpha}{R}\right) \\ -R\sin\left((s_0 + \mathrm{L_p} + \mathrm{L_{loop}} - s)\frac{\cos\alpha}{R}\right) \end{pmatrix}, \end{array} \tag{5.20}$$

with R and α the plectoneme radius and angle, $\mathrm{L_p}$ the contour length of DNA in the plectoneme and $\mathrm{L_{loop}}$ the contour length of the end loop. The starting orientation depends on the homoclinic solution and is set by s_0. The local unit tangent is $\mathbf{t}(s) = \dot{\mathbf{r}}(s)$. To simplify the calculations, we mention that the relation of the radius to the homoclinic parameter, as follows from equation (5.18), can be approximated in the relevant range $t \in [0.80424, 1)$ to

ample accuracy by:

$$t = 1 - 0.3799\left(\frac{R}{\lambda} + 0.0112\right)^2 \tag{5.21}$$

One often assumes the plectoneme to have a constant writhe per contourlength of

$$\omega = \frac{\sin(2\alpha)}{4\pi R} \tag{5.22}$$

although it is usually considered to be right within some approximation [153, 162] neglecting endloop and tails. In appendix (B) we show this expression to be exact when we include the change of writhe of the endloop while increasing the plectoneme length.

5.4.2 Elasticity

The free energy density (the free energy per length of strand) of the plectoneme has three distinct contributions: an elastic contribution due to the curved path of the centerline of DNA, an electrostatic repulsion of the two strands and a potential part due to the work done against the stretching force, which is just $\mathrm{f\,L_p}$. Since the curvature of a strand in the plectoneme is constant, the reduced elastic energy density is given by

$$\mathfrak{e}_{\mathrm{bend}}(t,\alpha) = \frac{\mathrm{P_b}}{2}\frac{\cos^4(\alpha)}{R(t)^2} \tag{5.23}$$

5.4.3 Electrostatics

Since DNA is a strong electrolyte, in a neutral pH environment, the persistence length gets an electrostatic correction. Using OSF theory [157, 158] and taking counterion condensation [163] into account by reducing the charge density along the chain to the charge density left after condensation [160], the resulting renormalized persistence length becomes:

$$\mathrm{P_b} = \mathrm{P_{b(0)}} + \frac{1}{4\kappa^2 Q_B} \tag{5.24}$$

with κ^{-1} the Debije screening length: and Q_B the Bjerrum length [164]:

$$\kappa = \sqrt{\frac{2q_e^2 n_s}{\epsilon_r \epsilon_0\,\mathrm{k_B T}}} \qquad\qquad Q_B = \frac{q^2}{4\pi\epsilon_r\epsilon_0\,\mathrm{k_B T}} \tag{5.25}$$

with ϵ_0 the electric constant, ϵ_r the dielectric constant of water, q_e the elementary charge and n_s the number density of salt molecules. For water at room temperature, 298 K, the Bjerrum length is 0.715 nm. Expressing the concentration of salt, c_s in mM(milli molar) or mol/ m^3

the inverse screening length at room temperature is $\kappa = 0.1\sqrt{c_s}$. The reduced energy density of the electrostatic interaction is described by the Ubbink-Odijk theory [153]:

$$\mathfrak{e}^0_{\mathrm{el}}(t,\alpha) = \frac{{\mathrm{q_{eff}}}^2\, Q_B}{2}\sqrt{\frac{\pi}{\kappa R(t)}}e^{-2\kappa R(t)} Z\,(\cot(\alpha)) \tag{5.26}$$

$$Z(x) = 1 + m_1 x^2 + m_2 x^4 \qquad m_1 = 0.828, m_2 = 0.864 \tag{5.27}$$

valid for $\cot(\alpha) < 1$, with $\mathrm{q_{eff}}$ the effective charge density of the centerline of a cylinder that is the source of a Debije-Hückel potential that coincides asymptotically in the small potential, far field with the nonlinear Poisson-Boltzmann potential of that cylinder with a given surface charge. For dsDNA we take a naked charge density of 2 charges per 0.34 nm, representing the 2 phosphate charges per basepair, and a radius of 1 nm.

The expansion is a fit that behaves reasonably also for $\cot\alpha$ close to one, where a standard asymptotic expansion would fail.

To calculate the effective charge density we follow the method laid out by Philip and Wooding [165]. It is fast and accurate for our conditions, plus it automatically gives the radius R^*, where the reduced potential equals 1 and thus the linearized theory breaks down. In Figure 5.4 and Figure 5.5 the dependence of the effective charge density and the non-linear radius R^* on the salt concentration are plotted for DNA. Note that the effective charge

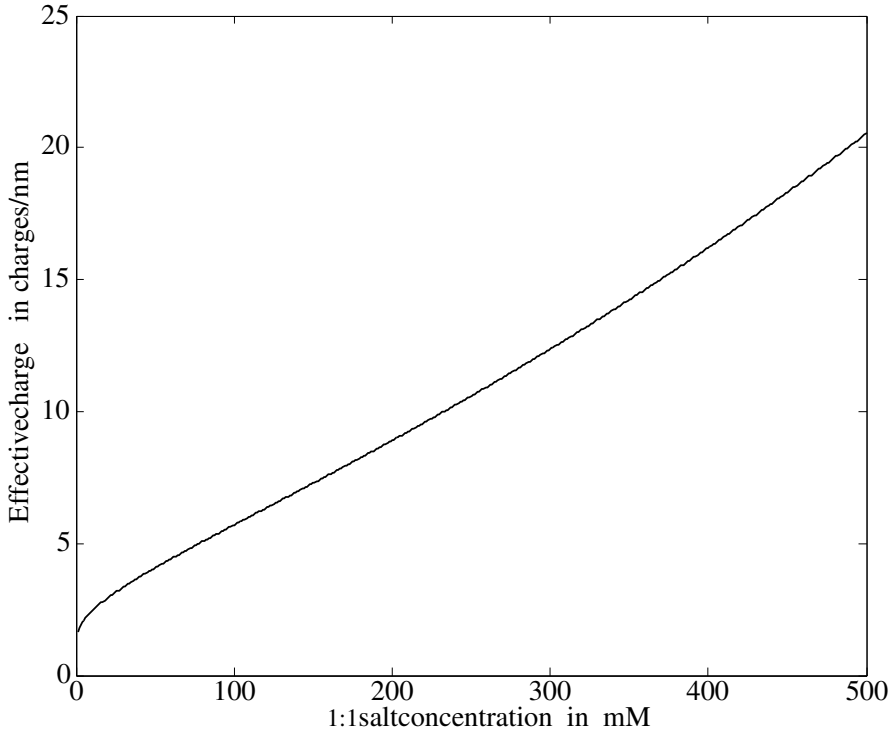

Figure 5.4: The effective charge line density as function of salt concentration

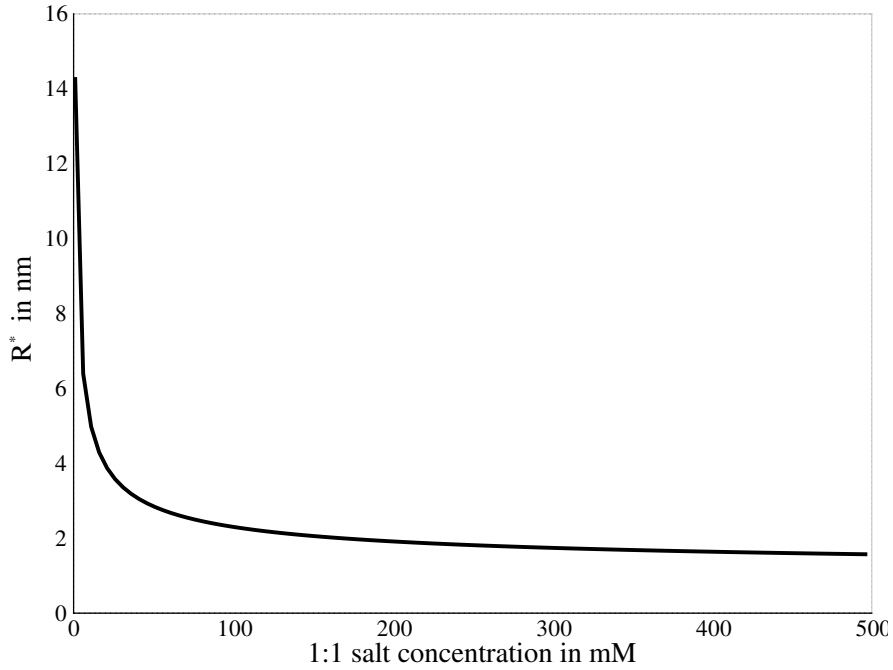

Figure 5.5: The radius where the electrostatic and thermal energy are equal as function of salt concentration

increases almost linearly with increasing salt concentration. This increase is a compensation for pushing back the charge to the centerline under stronger screening.

To understand the limitations it is good to recapitulate the limits of validity for the mean force calculations [166, 167] that form the basis of the treatment by Ubbink et al. First of all a mean field treatment with point like particles, that is Poisson-Boltzmann, needs to be applicable. That requirement is fulfilled since we are only looking at monovalent salt solutions[1]. The distance should be so large that within the nonlinear region around one cylinder, the potential of the other cylinder is negligible and, which in our case is practically equivalent, the potential halfway in between the two cylinders is small enough that linear superposition holds. We will see that under experimental conditions this requirement is fulfilled.

[1]See for a recent assessment [168])

5.4.4 Summing up

We have now an expression for the energy of a configuration with plectoneme under fixed linking number but still without thermal fluctuations:

$$\mathcal{E}(t,\alpha) = -\,\mathrm{f}(\mathrm{L_c}-\mathrm{L_p}) + \mathfrak{E}_{\mathrm{loop}}(t) + \mathrm{L_p}(\mathfrak{e}_{\mathrm{bend}}(t,\alpha) + \mathfrak{e}^0_{\mathrm{el}}(t,\alpha)) + \frac{(2\pi)^2\,\mathrm{P_c}}{2\,\mathrm{L_c}}\left(\mathrm{Lk}-\mathrm{Wr}_{\mathrm{loop}}(t)-\mathrm{L_p}\,\omega(t,\alpha)\right)^2 \quad (5.28)$$

For a plectoneme to form, a balance is needed between maximizing ω and minimizing the elastic, electrostatic, and potential free energy densities. The optimal plectoneme angle will settle between $\pi/4$, maximizing the writhe density, and $\pi/2$ minimizing bending energy. This is confirmed by explicit minimizations in Chapter 8. A condition for a local minimum to exist is that equation (5.28) has a minimum with respect to variations in $\mathrm{L_p}$ for finite positive $\mathrm{L_p}$:

$$\mathrm{L_p}(t,\alpha) = \frac{\mathrm{Lk}-\mathrm{Wr}_{\mathrm{loop}}(t)}{\omega(t,\alpha)} - \frac{\mathrm{L_c}}{(2\pi)^2\omega^2(t,\alpha)\,\mathrm{P_c}}(\mathfrak{e}_{\mathrm{bend}}(t,\alpha) + \mathfrak{e}^0_{\mathrm{el}}(t,\alpha) + \mathrm{f}) > 0. \quad (5.29)$$

The plectoneme is a global minimum when the resulting energy is lower than the straight chain solution. This second condition happens in general at larger Lk and so the transition is from a straight solution to a plectoneme with finite length. This *transition point*, when the global free energy minimum changes from the rod like solution to a plectoneme, is under usual experimental conditions considerably below the bifurcation point. The energy barrier between the two minima is of the order of $f\lambda \sim 10k_BT$, for lengths ($\sim 700-4000$nm) and forces ($\sim 1-4$pN) as used in the experiments. This results in a seemingly first order transition even at finite temperatures, rendering the behavior essentially different from the Euler buckling of semiflexible polymers, where thermal fluctuations destroy long range ordering as discussed in Chapter 3 without the addition of frictional forces [169].